Carbon Nanotube-Loaded Electrospun LiFePO$_4$/Carbon Composite Nanofibers As Stable and Binder-Free Cathodes for Rechargeable Lithium-Ion Batteries

Ozan Toprakci, Hatice A.K. Toprakci, Liwen Ji, Guanjie Xu, Zhan Lin, and Xiangwu Zhang*

Fiber and Polymer Science Program, Department of Textile Engineering, Chemistry and Science, North Carolina State University, 2401 Research Drive, Raleigh, NC, 27695-8301, United States

ABSTRACT: LiFePO$_4$/CNT/C composite nanofibers were synthesized by using a combination of electrospinning and sol–gel techniques. Polyacrylonitrile (PAN) was used as the electrospinning media and carbon source. Functionalized CNTs were used to increase the conductivity of the composite. LiFePO$_4$ precursor materials, PAN and functionalized CNTs were dissolved or dispersed in $N,N-$dimethylformamide separately and they were mixed before electrospinning. LiFePO$_4$ precursor/CNT/PAN composite nanofibers were then heat-treated to obtain LiFePO$_4$/CNT/C composite nanofibers. Fourier transform infrared spectroscopy measurements were done to demonstrate the functionalization of CNTs. The structure of LiFePO$_4$/CNT/C composite nanofibers was determined by X–ray diffraction analysis. The surface morphology and microstructure of LiFePO$_4$/CNT/C composite nanofibers were characterized using scanning electron microscopy and transmission electron microscopy. Electrochemical performance of LiFePO$_4$/CNT/C composite nanofibers was evaluated in coin-type cells. Functionalized CNTs were found to be well-dispersed in the carbonaceous matrix and increased the electrochemical performance of the composite nanofibers. As a result, cells using LiFePO$_4$/CNT/C composite nanofibers have good performance, in terms of large capacity, extended cycle life, and good rate capability.

KEYWORDS: lithium-ion batteries, cathodes, LiFePO$_4$, carbon nanofibers, carbon nanotubes
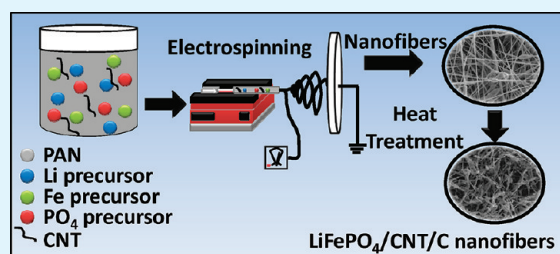
1. INTRODUCTION

Rapidly increasing demand for lithium-ion batteries opened a new area in the cathode material research. Among various cathode materials, lithium iron phosphate (LiFePO$_4$) comes into prominence because of its high discharge potential, excellent cycling performance, good thermal stability, low toxicity, relatively low cost, and safe nature. However, LiFePO$_4$ has low conductivity ($\sim 1 \times 10^{-9}$ S cm^{-1}), which causes poor rate capability and high impedance.[1] To increase the efficiency of LiFePO$_4$, researchers proposed various structural and morphological modifications such as doping LiFePO$_4$ with metal ions,[1-3] reducing the particle size,[4,5] coating with conductive materials,[6-8] and fabrication of conductive LiFePO$_4$ composites.[9-15] In all these methods, conductive LiFePO$_4$ composites are of increasing importance for their contribution to electrochemical performance. These materials are typically prepared by mixing LiFePO$_4$ or its precursors with a polymer, followed by a heat treatment procedure to convert the polymer matrix into a conductive carbon. The conductivity of these composites can be further improved by adding additional electrical conductors. Although many materials can be used to increase the electrical conductivity of the system,[14,16,17] carbon nanotubes (CNTs) are one of the most promising materials because of their high electrical conductivity, large surface area, and high aspect ratio.[18,19]

LiFePO$_4$ is typically produced by both solid-state and solution-based methods, which have been reviewed else-

where.[20-23] In this work, LiFePO$_4$/CNT/C composite nanofibers were synthesized via the combination of electrospinning and sol–gel techniques. The novelty of this study mainly stems from the unique electrospinning process. Electrospun precursor/CNT/polyacrylonitrile (PAN) nanofibers can be easily converted into LiFePO$_4$/CNT/C composite nanofibers by heat treatment. After heat treatment, the resultant LiFePO$_4$/CNT/C composite nanofibers form free-standing and flexible mats that not only show increased electrical conductivity but also eliminate the use of polymer binders. The unique composite nanofiber structure also restricts the growth of LiFePO$_4$ particles during heat treatment. Because the transformation of PAN to carbon and formation of LiFePO$_4$ particles take place simultaneously in composite nanofibers, the carbon nanofiber matrix behaves as an inhibitor between the LiFePO$_4$ particles and prevents the particle growth. This further shortens the charge transfer distance and leads to increased lithium diffusion coefficient. Thus, LiFePO$_4$/CNT/C composite nanofibers can not only have large capacity and good cycling performance but also possess high rate capability. In addition, chemically modified CNTs are incorporated into the composite nanofibers in order to enhance the electrochemical performance and the stability of the LiFePO$_4$ cathodes. As schematically presented in

Figure 1, homogeneously dispersed CNTs can form conducting bridges between LiFePO$_4$ particles and increase the electrical
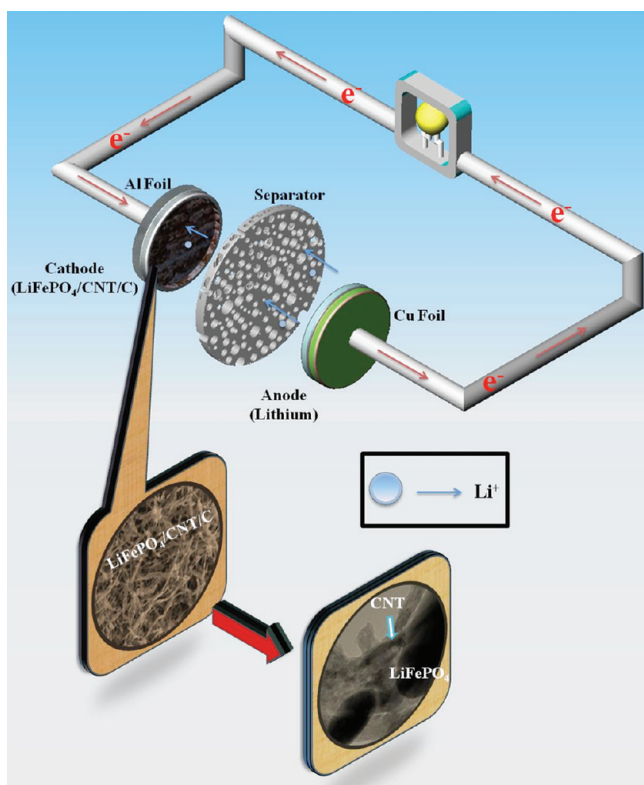
Figure 1. Schematic diagram of LiFePO$_4$/CNT/C composite nanofibers as cathodes for lithium-ion batteries.

conductivity of the system. Here, we present the preparation, structure, morphology, and electrochemical performance of electrospun LiFePO$_4$/CNT/C composite nanofiber cathodes for lithium-ion batteries.

2. MATERIALS AND METHODS

2.1. Functionalization of CNTs. Multiwalled CNTs with purity of 95 wt % were purchased from Nanostructured & Amorphous Materials, Inc. These CNTs are about 10−20 nm in diameter and 10−30 μm in length with an approximate surface area of 500 m^2 g^{-1}. As shown in Figure 2a, CNTs are found in entangled bundles caused by high level of van der Waals interactions between them. In addition, these CNTs have inert, stable structure because of the sp^2 hybridized carbon atoms.[18] To increase the filler−matrix interaction and ensure good filler dispersion in the matrix, we chemically modified CNTs before use.

Before the chemical modification, purification was carried out according to ref 10. To remove the catalyst, we treated CNTs with diluted sulfuric acid (50 wt %) at 140 °C for 3 h. Then, CNTs were filtered by using glass frit, washed with distilled water, and dried at 120 °C for 12 h. Purified CNTs were functionalized as described by Zhang et al.[24] First, 0.01 g of purified CNTs were oxidized in 100 mL of HNO$_3$ and H$_2$SO$_4$ mixture (1:3 by volume) solution by refluxing at 70 °C for 8 h and sonicated for 4 h to prepare carboxylic acid-functionalized CNTs (CNT-COOH). Then, the solution was filtered by vacuum filtration through a poly(tetrafluoroethylene) (PTFE) filter (Millipore, 25 mm in diameter, 0.2 μm pores) and washed with distilled water. In the next step, CNT−COOH mixture was treated with SOCl$_2$ (Fisher) at 65 °C for 24 h to obtain CNT−COCl, which was then mixed with Triton X−100 (EMD Chemicals) in *N,N*−dimethylformamide (DMF, Aldrich) and treated at 120 °C for 48 h under N$_2$ atmosphere. Functionalized CNTs (i.e., CNT-Triton X)
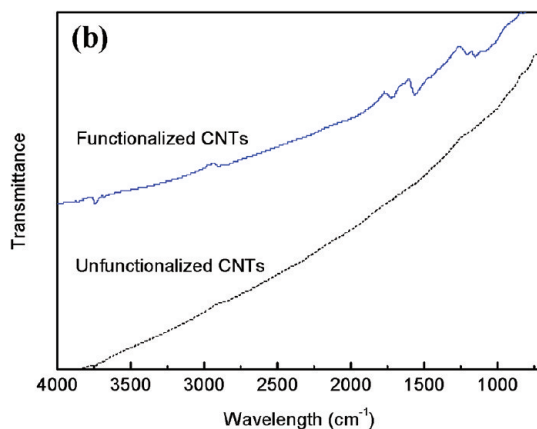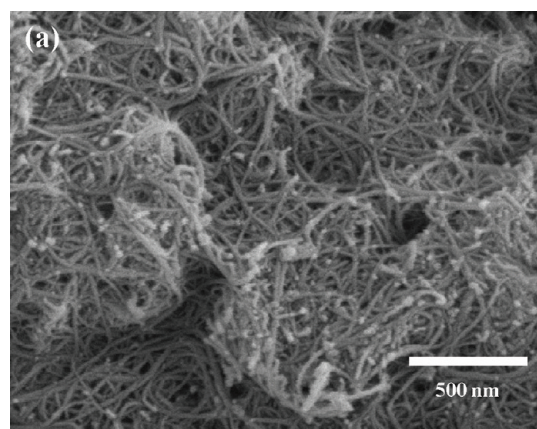

Figure 2. (a) SEM image of as-received CNTs, and (b) FT-IR spectra of unfunctionalized and functionalized CNTs.

were filtered, washed with distilled water, and dried at room temperature for 24 h. Fourier transform infrared spectroscopy (FT−IR, Thermo Nicolet, Nexus 470) was used to demonstrate the functionalization of CNTs in ATR mode. The tests were carried out in the range between 700−4000 cm^{-1} and FT-IR data were obtained by averaging 64 scans at a resolution of 4 cm^{-1}.

2.2. Preparation of Composite Nanofibers. Electrospun LiFePO$_4$/CNT/C composite nanofibers were prepared as cathode materials for lithium-ion batteries. Spinning solutions consisted of polyacrylonitrile (PAN, Pfaltz & Bauer Inc., 150,000 g mol^{-1}), functionalized CNTs, and LiFePO$_4$ precursor. PAN was used not only for the spinning media but also as the carbon source. PAN was first dissolved in DMF at room temperature by stirring for 24 h. For LiFePO$_4$ precursor, lithium acetate (LiCOOCH$_3$, Aldrich), phosphoric acid (H$_3$PO$_4$, Aldrich) and iron(II) acetate (Fe(COOCH$_3$)$_2$, Aldrich) were used as the starting materials and mixed in DMF at a stoichiometric ratio of 1:1:1 by stirring at room temperature for 24 h. Functionalized CNTs were dispersed in DMF. Separately prepared CNT, PAN, and LiFePO$_4$ precursor solutions were then mixed and the concentrations of each component are given in Table 1.

Table 1. Concentrations of LiFePO$_4$ Precursor, PAN, and CNT in Electrospinning Solutions

sample ID	LiFePO$_4$ precursor (wt%)	PAN (wt %)	functionalized CNT (wt %)
LiFePO$_4$ precursor/ PAN	8	4	0
LiFePO$_4$ precursor/ CNT/PAN	8	4	0.1

1274

dx.doi.org/10.1021/am201527r | *ACS Appl. Mater. Interfaces* 2012, 4, 1273−1280
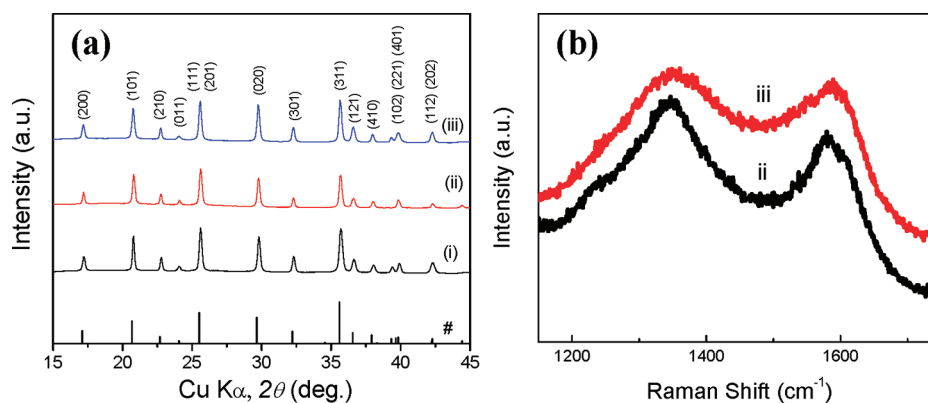
Figure 3. (a) X-ray diffraction patterns and (b) Raman spectra of (i) pristine $LiFePO_4$ powder, (ii) $LiFePO_4$/C composite nanofibers, and (iii) $LiFePO_4$/CNT/C composite nanofibers. #: The reflections of $LiFePO_4$ (ICDD No. 96-110-1112) are shown for comparison.

Electrospinning solutions were placed in 10 mL syringes with metal needles of 0.012 in. in diameter. A variable high voltage power supply (Gamma ES40P−20W/DAM) was used to provide a high voltage (around 14 kV) for electrospinning with 0.5 ml h^{-1} flow rate and 15 cm needle-to-collector distance. The electrospun $LiFePO_4$ precursor/CNT/PAN composite nanofibers were first stabilized in air environment at 280 °C for 5 h (heating rate was 5 °C min^{-1}) and then calcinated/carbonized at 700 °C for 18 h in argon atmosphere (heating rate was 2 °C min^{-1}). Heat-treatment conditions were inclusively discussed in previous studies.[15,25,26] For comparison, electrospun $LiFePO_4$/C composite nanofibers were prepared without adding CNTs. Pristine $LiFePO_4$ powder was also prepared by using the sol−gel method described in ref 27.

2.3. Structural and Morphological Characterization. The structural characterization of $LiFePO_4$/C and $LiFePO_4$/CNT/C composite nanofibers was carried out by small-angle X-ray diffraction (SAXD, Rigaku Smartlab X−Ray Diffraction System, Cu Kα, λ = 1.5405 Å) in a 2θ range of 5−60°, with 2θ step-scan intervals of 0.05°. The structural variations of carbonaceous material in the composite nanofibers were identified by Raman spectroscopy (Horiba Jobin Yvon LabRam Aramis Microscope, 633 nm HeNe Laser). The carbon contents of composite nanofibers were determined by elemental analysis (Perkin Elmer 2400 Series II CHNS/O Elemental Analyzer). The morphology and diameter of heat-treated electrospun fibers and pristine $LiFePO_4$ powder were evaluated by using field emission scanning electron microscope (FESEM−JEOL 6400F SEM at 5 kV). The microstructure of heat-treated $LiFePO_4$/CNT/C composite nanofibers was also observed using transmission electron microscope (Hitachi HF2000 TEM at 200 kV). Before TEM observation, samples were ultrasonically treated in a solution of ethanol and then deposited on 200-mesh carbon-coated copper grids.

2.4. Electrochemical Measurements. $LiFePO_4$/C and $LiFePO_4$/CNT/C composite nanofibers were directly used as binder-free cathodes for electrochemical measurements. For pristine $LiFePO_4$ powder, a mixture of 80 wt % active material, 10 wt % PVDF binder (Acros Organics, 1,300,000 g mol^{-1}) and 10 wt % carbon black was dispersed in N-methyl-2-pyrrolidone (Aldrich). The obtained slurry was casted on aluminum foil and dried in vacuum at 120 °C for 24 h. CR2032−type coin cells (diameter = 20 mm and height = 3.2 mm) were fabricated using lithium metal as the counter electrode in an argon-filled glove box. The cathode weight was around 2.5 mg per electrode. The electrolyte used consisted of 1 M solution of $LiPF_6$ in a mixture (1:1 by volume) of ethylene carbonate (EC) and diethyl carbonate (DEC). The separator (Celgard 480) was soaked in the electrolyte for 24 h prior to testing.

Electrochemical impedance spectrum (EIS) measurements were performed using a frequency response analyzer (Gamry Reference 600 Potentiostat) in a frequency range of 1 MHz to 0.001 Hz and a potentiostatic signal amplitude of 10 mV s^{-1}. The charge and discharge characteristics of the cathodes were evaluated at various current rates (0.05−2C, 1C = 170 mA g^{-1}) in the range of 2.5−4.2 V versus Li/Li$^+$.

All electrochemical experiments were conducted at room temperature and all capacity values were calculated based on the weight of active material $LiFePO_4$.

3. RESULTS AND DISCUSSION

3.1. Structural and Morphological Characterization of Pristine $LiFePO_4$ Powder, and $LiFePO_4$/C and $LiFePO_4$/CNT/C Composite Nanofibers. Figure 2b shows the FT−IR spectra of purified CNTs and functionalized CNTs (i.e., CNT-Triton X). It is seen that in functionalized CNTs, new peaks occur at around 1240 and 1110 cm^{-1}, which indicate that Triton X has been successfully grafted onto the CNT surface. As previously reported,[24] these peaks were determined as C−O belonged to ester and C−O bonds occurred during the reaction between carboxylic acid and Triton X, respectively. In addition, new bands also appear around 1500−1600 cm^{-1}, which can be assigned to C═C bonding and attributed to the formation of electric dipoles caused by disruption of nanotube symmetry during surface modification.[28]

Figure 3a shows the XRD patterns of pristine $LiFePO_4$ powder, $LiFePO_4$/C composite nanofibers, and $LiFePO_4$/CNT/C composite nanofibers produced at 700 °C for 18 h. The lattice parameters of all samples are the same to those given in the ICDD card (No. 96−110−1112).[29] It is seen that all diffraction peaks of pristine $LiFePO_4$ powder, $LiFePO_4$/C composite nanofibers, and $LiFePO_4$/CNT/C composite nanofibers can be indexed to an olivine $LiFePO_4$ with orthorhombic crystal structure (space group *Pnma*) and there are no impurity phase peaks. From Figure 3a, it is also seen that $LiFePO_4$/C and $LiFePO_4$/CNT/C composite nanofibers show broader olivine peaks with lower intensities, as compared with pristine $LiFePO_4$ powder. This is because the presence of carbon in the fiber structure slows down the crystal-growth during heat-treatment.[15] From Figure 3a, the average $LiFePO_4$ crystallite size, which is different than particle size, can be calculated by the Scherrer's equation ($L = 0.9\lambda/\beta\cos\theta$) from the full width at half maximum (FWHM or β) of (2 0 0), (1 0 1), (2 0 1) or (1 1 1), (0 2 0), and (3 1 1) peaks.[30] Crystallite sizes for pristine $LiFePO_4$ powder, and $LiFePO_4$/C and $LiFePO_4$/CNT/C composite nanofibers were calculated to be 45, 38, and 37 nm, respectively.

Figure 3b shows Raman spectra of $LiFePO_4$/C and $LiFePO_4$/CNT/C composite nanofibers. Both nanofibers show well-known D-band (disorder-induced phonon mode) in the range of 1250−1450 cm^{-1} and G-band (graphite band) between 1550 and 1660 cm^{-1}. The peak at around 1350 cm^{-1} is
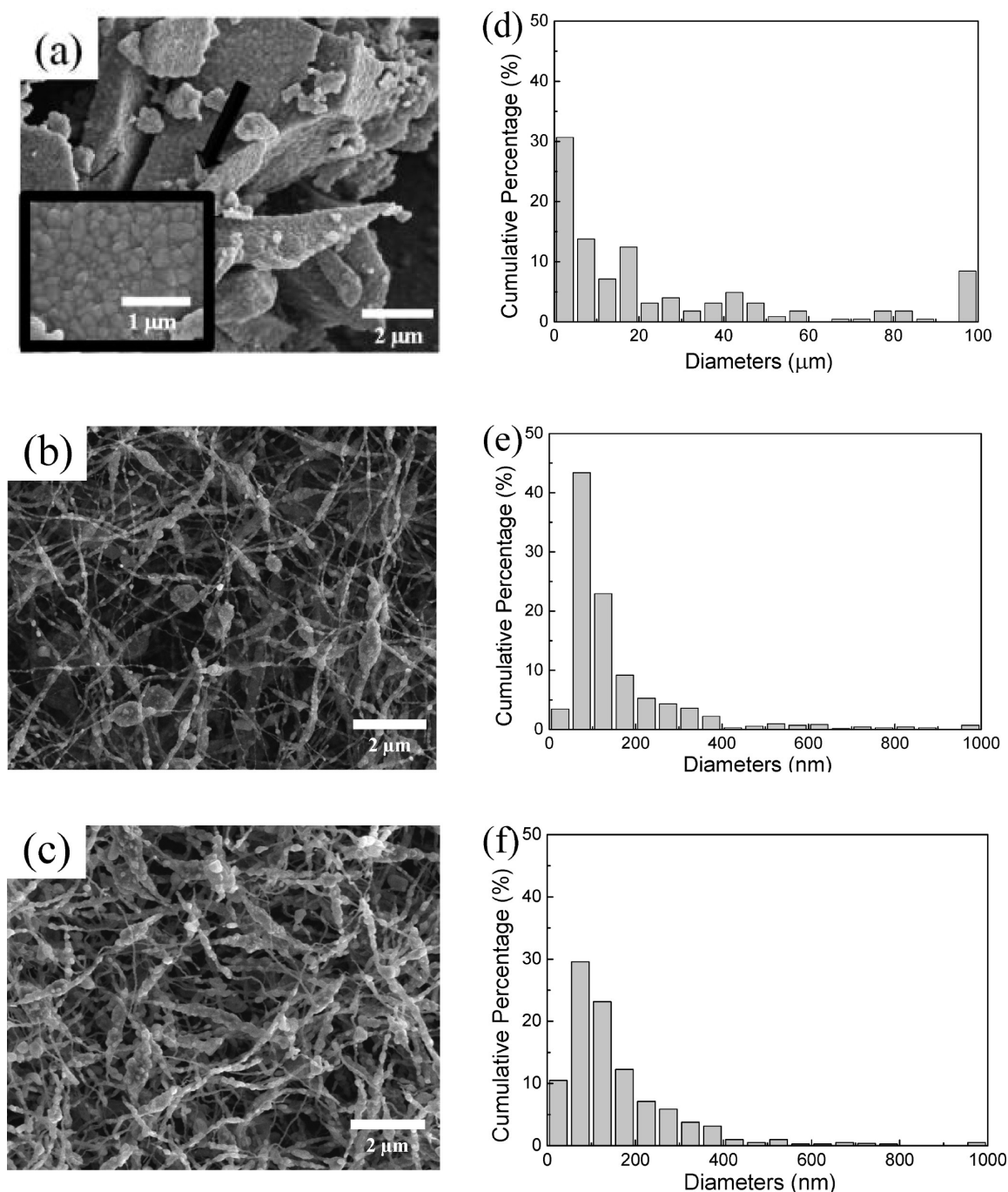
Figure 4. SEM images and diameter distributions of (a, d) pristine LiFePO$_4$ powder, (b, e) LiFePO$_4$/C composite nanofibers, and (c, f) LiFePO$_4$/CNT/C composite nanofibers.

attributed to defects and disordered portions of carbon (sp^3-coordinated) and the peak at around 1600 cm^{-1} is indicative of ordered graphitic crystallites of carbon (sp^2-coordinated). The relative intensities (I_D/I_G) can be used to analyze the amount of carbon defects in the CNFs. Lower I_D/I_G ratio indicates the presence of larger amount of sp^2-coordinated carbon.[31−35] As shown in Table 2, I_D/I_G ratio decreases from 1.165 to 1.049 with the addition of CNTs in the precursor. Therefore, composite nanofibers without CNTs contain higher amount of disordered sections and defects. This also demonstrates that the presence of CNTs helps to create more ordered carbon in nanofibers.

The carbon contents of heat-treated products were measured by using elemental analysis and they were found to be 0.75, 22.8, and 25.4 wt %, respectively, for pristine LiFePO$_4$ powder, LiFePO$_4$/C composite nanofibers, and LiFePO$_4$/CNT/C composite nanofibers.

Table 2. Characteristic Raman Bands of LiFePO$_4$/C and LiFePO$_4$/CNT/C Composite Nanofibers

sample	D peak (cm^{-1})	G peak (cm^{-1})	I_D/I_G value
LiFePO$_4$/C	1346	1579	1.165
LiFePO$_4$/CNT/C	1360	1589	1.049

SEM images and diameter distributions of the pristine LiFePO$_4$ powder, LiFePO$_4$/C composite nanofibers, and LiFePO$_4$/CNT/C composite nanofibers are shown in Figure 4, respectively. As shown in Figure 4a, pristine LiFePO$_4$ powder shows primary particle size in the range of 55−350 nm with an average of 197 nm. Although the primary particle size seems to be low, it is apparent that they form agglomerates in the range of 1−175 μm with an average of 32 μm, which is an obstacle for electrolyte penetration. The size distribution of pristine LiFePO$_4$ powder is shown in Figure 4d.

As shown in images b and c in Figure 4, both LiFePO$_4$/C and LiFePO$_4$/CNT/C composite nanofibers kept their "networklike" structures after heat treatment. Comparing with Figure 4a, it can be found that the nanofiber structure restricts the agglomeration of LiFePO$_4$ particles. During heat treatment, PAN matrix was converted to carbon, and at the same time, it prevented the formation of large aggregates of LiFePO$_4$ particles and ensured the homogeneous carbon coating on the surface of LiFePO$_4$ particles. From panels e and f in Figure 4, slight differences in the fiber diameter and diameter distribution can be observed. Although the average fiber diameter is 160 nm for LiFePO$_4$/C, it increases to 168 nm for LiFePO$_4$/CNT/C composite nanofibers. This may be caused by the increase in solution viscosity due to the addition of CNTs. Typically, higher solution viscosity results in larger fiber diameter due to the greater resistance of the solution to the stretching force caused by the charges in the electrospun jet.[15,36−39]

Figure 5 represents TEM images of LiFePO$_4$/CNT/C composite nanofibers at different magnifications. As shown in
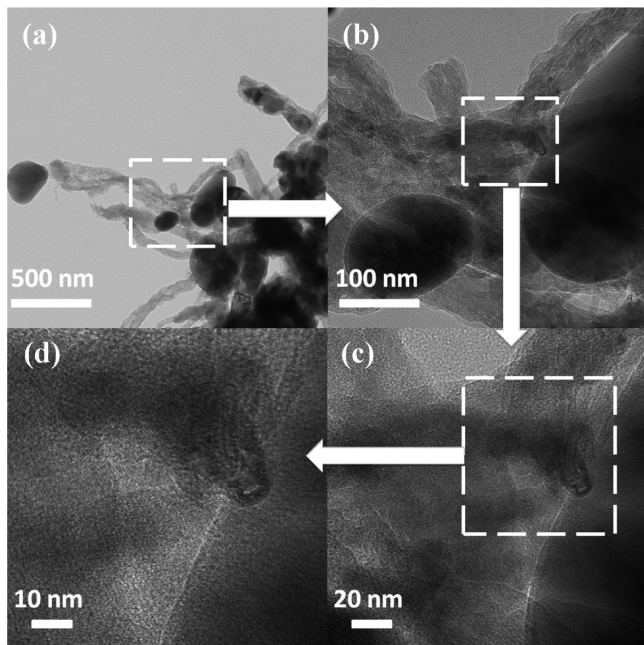
Figure 5. TEM images of LiFePO$_4$/CNT/C composite nanofibers at various magnifications: (a) 20 000×, (b) 80 000×, (c) 200 000×, and (d) 400 000×.

Figure 2b, CNTs have been successfully functionalized, which provides higher interaction with PAN matrix. The functionalization of CNTs leads to the separation of CNTs bundles and homogeneous dispersion throughout the composite.[40,41] LiFePO$_4$/CNT/C composite nanofibers consist of two types of conductors: carbon fiber matrix and CNTs. CNTs have higher electrical conductivity mainly due to their unique graphite wall structure.[19] Well-dispersed CNTs can easily form a conducting network throughout the composite even at low concentrations because of their high aspect ratio.[40,41] As shown in Figure 5, functionalized CNTs form bridges between LiFePO$_4$ particles, which play an important role in enhancing the electron transport throughout the composite.[42] As shown in panels a and b in Figure 2, CNTs are found in bundles. From images c and d in Figure 5, it is seen that CNTs were successfully modified and separated from each other, which might be an indication of good distribution. From both SEM and TEM images, it is obvious that electrospinning is an effective way of minimizing the particle aggregation. During heat treatment, the transformation of PAN matrix to carbon leads to the formation of conductive layer on LiFePO$_4$ particles, increases the particle-to-particle distance, and prevents the particle aggregation. As shown in Figure 5c, the carbonaceous layer is as thin as 3 nm, which is beneficial for the penetration of Li ions.

3.2. Electrochemical Performance of Pristine LiFePO$_4$ Powder, and LiFePO$_4$/C and LiFePO$_4$/CNT/C Composite Nanofibers. EIS measurements were carried out in the frequency range from 1 mHz to 1 MHz with an AC voltage signal of ±5 mV for pristine LiFePO$_4$ powder, LiFePO$_4$/C composite nanofibers, and LiFePO$_4$/CNT/C composite nanofibers. Prior to the EIS measurements, cells were firstly activated by five charge/discharge cycles at 0.05 C between 2.5 V and 4.2 V vs. Li/Li$^+$, and then they were polarized to 3.4 V. The potential was maintained for 5 h for the formation of a stable solid-electrolyte interface (SEI) film at the surface of the cathode.[16] Figure 6a illustrates the typical Nyquist plots of pristine LiFePO$_4$ powder, LiFePO$_4$/C composite nanofibers, and LiFePO$_4$/CNT/C composite nanofibers. The amplification of the high and medium frequency regions is also shown in Figure 6b. The intercept of the curve in high frequency to the real axis relates to the ohmic resistance of electrolyte (R_Ω). The depressed semicircle in the medium-frequency region is related to the charge transfer resistance (R_{ct}) at the particle surface. The increase in the semicircle radius indicates the increase in charge transfer resistance. The straight line in the low-frequency region is related to the diffusion behavior of lithium ions within the LiFePO$_4$ particles or also called Warburg resistance (Z_w).[43−47]

From Figure 6, charge transfer resistance (R_{ct}) values were calculated to be 7360, 960.2, and 607.6 Ω, respectively, for pristine LiFePO$_4$ powder, LiFePO$_4$/C composite nanofibers, and LiFePO$_4$/CNT/C composite nanofibers. Among all samples, LiFePO$_4$/CNT/C composite nanofibers have the lowest R_{ct} value, indicating that these nanofibers possess better reaction kinetics of lithium ion insertion/extraction during electrochemical cycling than those of LiFePO$_4$/C composite nanofibers and pristine LiFePO$_4$ powder. The small charge transfer resistance of LiFePO$_4$/CNT/C composite nanofibers can be related to decreased particle size and relatively high carbon content.[44,46]

Figure 7a shows the cycling performance of pristine LiFePO$_4$ powder, LiFePO$_4$/C composite nanofibers, and LiFePO$_4$/CNT/C composite nanofibers at a constant current density of 8.5 mA g^{-1} (or 0.05 C). During the first three cycles, instead of capacity fading, a slight increase in discharge capacity occurs for pristine LiFePO$_4$ powder and LiFePO$_4$/C composite nanofibers. This can be attributed to the slow electrolyte penetration into the electrodes or the crack formation on the
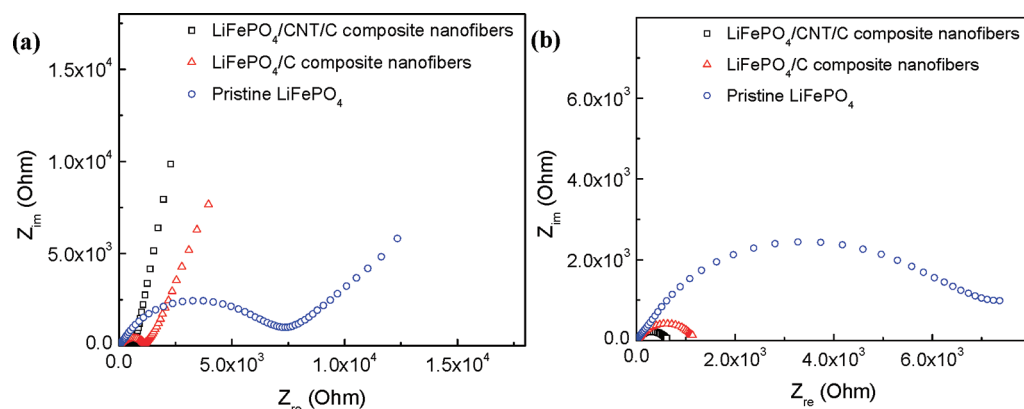
Figure 6. (a) Electrochemical impedance curves of pristine LiFePO$_4$ powder, LiFePO$_4$/C composite nanofibers, and LiFePO$_4$/CNT/C composite nanofibers, and (b) amplification of medium- and high-frequency regions.
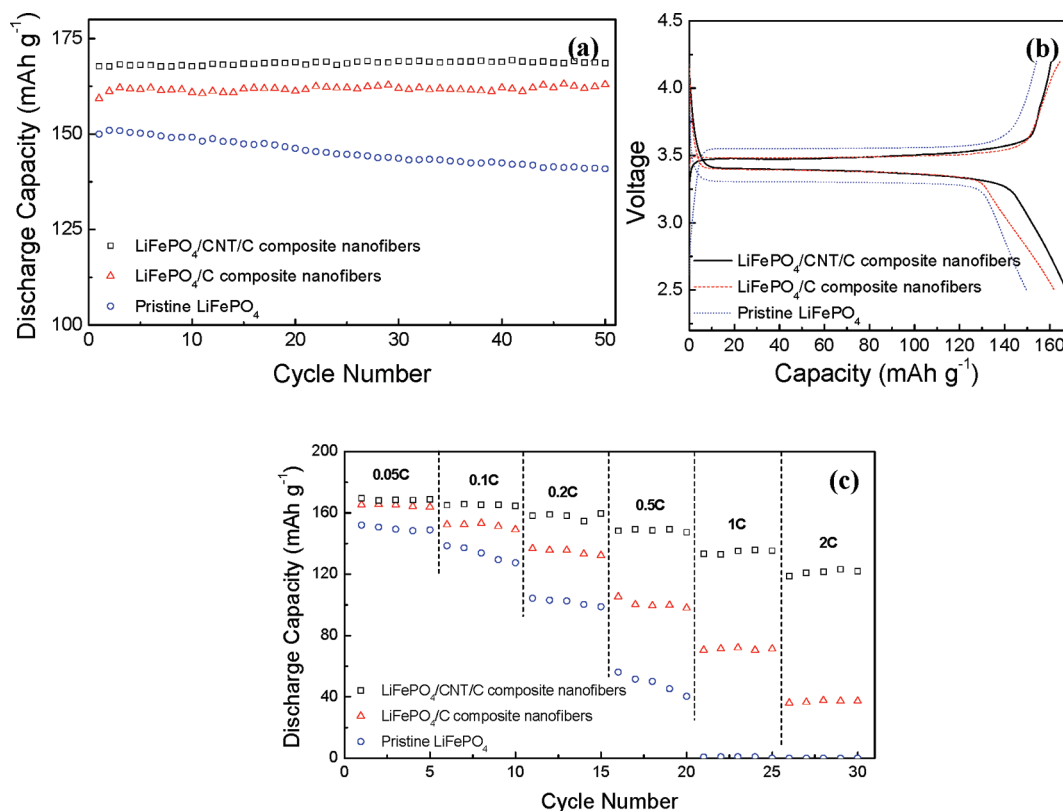
Figure 7. (a) Cycling performance, (b) initial voltage vs. capacity curves, and (c) rate capabilities of pristine LiFePO$_4$ powder, LiFePO$_4$/C composite nanofibers, and LiFePO$_4$/CNT/C composite nanofibers. Charge−discharge rate used in a and b was 0.05 C.

amorphous carbon layer during cycling, which increases the electrode surface area and enhances the electrode-electrolyte interaction.[7] From Figure 7a, it is also seen that the reversible capacities remain relatively constant for LiFePO$_4$/C and LiFePO$_4$/CNT/C composite nanofibers (i.e., 161 and 169 mA h g^{-1}, respectively) over the entire fifty cycles. These values correspond to 95 and 99% of the theoretical capacity of LiFePO$_4$. On the other hand, pristine LiFePO$_4$ powder shows a continuous capacity fading during fifty cycles. Reversible capacity of pristine LiFePO$_4$ powder decreases from 150 to 135 mA h g^{-1}, which corresponds to 90% capacity retention from the first cycle.

Typical charge/discharge curves of pristine LiFePO$_4$ powder, LiFePO$_4$/C composite nanofibers, and LiFePO$_4$/CNT/C composite nanofibers are shown in Figure 7b. The charge/

discharge curves were obtained at 0.05 C with a potential window of 2.5−4.2 V. It is seen that during the first cycle, LiFePO$_4$/C and LiFePO$_4$/CNT/C composite nanofibers show similar flat voltage plateaus at around 3.5 and 3.4 V, respectively, for charging and discharging, which are the characteristic behavior of the two-phase reaction of LiFePO$_4$. However, pristine LiFePO$_4$ powder shows higher polarization and its plateaus are at around 3.6 V (charging) and 3.3 V (discharging), respectively. From Figure 7b, it is also seen that initial reversible capacities are 150, 162, and 169 mA h g^{-1}, respectively, for pristine LiFePO$_4$ powder, LiFePO$_4$/C composite nanofibers and LiFePO$_4$/CNT/C composite nanofibers. The relatively good electrochemical performance of LiFePO$_4$/C and LiFePO$_4$/CNT/C composite nanofibers can be attributed to their unique one-dimensional fiber structure

and the effective lithium-ion transportation on the large nanofiber surface.

Figure 7c shows the rate capabilities of pristine LiFePO$_4$ powder, LiFePO$_4$/C composite nanofibers, and LiFePO$_4$/CNT/C composite nanofibers. During the tests, the nanofibers were charged at 0.05 C, but discharged at different C-rates. When the C-rate increases from 0.05 to 2 C (i.e., from 8.5 to 340 mA h g^{-1}), LiFePO$_4$/CNT/C composite nanofibers show satisfactory rate capability compared with LiFePO$_4$/C composite nanofibers and pristine LiFePO$_4$ powder. It can be inferred that CNTs play a significant role in improving the reaction kinetics of LiFePO$_4$, especially, at high discharge rates, and this is also consistent with EIS measurements (Figure 6). Average reversible capacities of LiFePO$_4$/CNT/C composite nanofibers are obtained as 169, 165, 158, 148, 134, and 121 mA h g^{-1}, respectively, for discharge rates of 0.05, 0.1, 0.2, 0.5, 1, and 2 C.

The excellent electrochemical performance of LiFePO$_4$/CNT/C composite nanofibers is mainly caused by their unique structure. Carbon nanofiber matrix creates a conductive networklike structure throughout the electrode. The carbon nanofiber matrix also has high surface-to-volume ratio, complex porous structure, and shortened lithium-ion diffusion pathway, which enhance the electrode reaction kinetics and reduce the polarization. LiFePO$_4$ particles embedded in the carbon nanofiber matrix have small size, which is also beneficial for achieving higher reversible capacities. In addition, the incorporation of functionalized CNTs helps to form conducting bridges between particles and provides higher electrochemical efficiency. Therefore, LiFePO$_4$/CNT/C composite nanofibers have good cycling performance, high reversible capacity, and excellent rate capability.

■ CONCLUSIONS

Electrospun LiFePO$_4$/C and LiFePO$_4$/CNT/C composite nanofibers were synthesized using electrospinning, followed by heat treatment. Electrospinning was found to be an effective way in minimizing the aggregation of LiFePO$_4$ particles and promoting the formation of a conducting carbonaceous layer on LiFePO$_4$ particle surface. Functionalized CNTs were found to be well-dispersed in the matrix and help increase the electrochemical performance of the LiFePO$_4$ cathodes by forming conducting bridges between LiFePO$_4$ particles and enhancing the electron transport of the system.

■ AUTHOR INFORMATION

Corresponding Author
*Tel.: +1 919 515 6547. Fax: +1 919 515 6532. E-mail: xiangwu_zhang@ncsu.edu.

Notes
The authors declare no competing financial interest.

■ ACKNOWLEDGMENTS

■ REFERENCES

(1) Chung, S.; Bloking, J. T.; Chiang, Y. *Nat. Mater.* **2002**, *1*, 123−128.

(2) Herle, P. S.; Ellis, B.; Coombs, N.; Nazar, L. F. *Nat. Mater.* **2004**, *3*, 147−152.

(3) Wang, D. Y.; Li, H.; Shi, S. Q.; Huang, X. J.; Chen, L. Q. *Electrochim. Acta* **2005**, *50*, 2955−2958.

(4) Delacourt, C.; Poizot, P.; Levasseur, S.; Masquelier, C. *Electrochem. Solid-State Lett.* **2006**, *9*, A352−A355.

(5) Milke, B.; Strauch, P.; Antonietti, M.; Giordano, C. *Nanoscale* **2009**, *1*, 110−113.

(6) Ravet, N.; Chouinard, Y.; Magnan, J. F.; Besner, S.; Gauthier, M.; Armand, M. *J. Power Sources* **2001**, *97-98*, 503−507.

(7) Dominko, R.; Bele, M.; Gaberscek, M.; Remskar, M.; Hanzel, D.; Goupil, J. M.; Pejovnik, S.; Jamnik, J. *J. Power Sources* **2006**, *153*, 274−280.

(8) Chen, Z. H.; Dahn, J. R. *J. Electrochem. Soc.* **2002**, *149*, A1184−A1189.

(9) Jin, B.; Gu, H.; Zhang, W.; Park, K.; Sun, G. *J. Solid State Electrochem.* **2008**, *12*, 1549−1554.

(10) Kavan, L.; Exnar, I.; Cech, J.; Graetzel, M. *Chem. Mat.* **2007**, *19*, 4716−4721.

(11) Liu, Y.; Li, X.; Guo, H.; Wang, Z.; Peng, W.; Yang, Y.; Liang, R. *J. Power Sources* **2008**, *184*, 522−526.

(12) Zhou, Y.; Wang, J.; Hu, Y.; O'Hayre, R.; Shao, Z. *Chem. Commun.* **2010**, *46*, 7151−7153.

(13) Ojczyk, W.; Marzec, J.; Swierczek, K.; Zajac, W.; Molenda, M.; Dziembaj, R.; Molenda, J. *J. Power Sources* **2007**, *173*, 700−706.

(14) Kim, C. W.; Park, J. S.; Lee, K. S. *J. Power Sources* **2006**, *163*, 144−150.

(15) Toprakci, O.; Ji, L.; Lin, Z.; Toprakci, H. A. K.; Zhang, X. *J. Power Sources* **2011**, *196*, 7692−7699.

(16) Wang, G. X.; Yang, L.; Chen, Y.; Wang, J. Z.; Bewlay, S.; Liu, H. K. *Electrochim. Acta* **2005**, *50*, 4649−4654.

(17) Bhuvaneswari, M. S.; Bramnik, N. N.; Ensling, D.; Ehrenberg, H.; Jaegermann, W. *J. Power Sources* **2008**, *180*, 553−560.

(18) Baughman, R. H.; Zakhidov, A. A.; de Heer, W. A. *Science* **2002**, *297*, 787−792.

(19) Ebbesen, T. W.; Lezec, H. J.; Hiura, H.; Bennett, J. W.; Ghaemi, H. F.; Thio, T. *Nature* **1996**, *382*, 54−56.

(20) Jugovic, D.; Uskokovic, D. *J. Power Sources* **2009**, *190*, 538−544.

(21) Toprakci, O.; Toprakci, H. A. K.; Ji, L.; Zhang, X. *KONA Powder Part. J.* **2010**, 50−73.

(22) Su, L.; Jing, Y.; Zhou, Z. *Nanoscale* **2011**, *3*, 3967−3983.

(23) Zhang, X.; Ji, L.; Toprakci, O.; Liang, Y.; Alcoutlabi, M. *Polym. Rev.* **2011**, *51*, 239−264.

(24) Zhang, Q.; Chang, Z.; Zhu, M.; Mo, X.; Chen, D. *Nanotechnology* **2007**, *18*, 115611.

(25) Ji, L.; Zhang, X. *Nanotechnology* **2009**, *20*, 155705.

(26) Bonino, C. A.; Ji, L.; Lin, Z.; Toprakci, O.; Zhang, X.; Khan, S. A. *ACS Appl. Mater. Interfaces* **2011**, *3*, 2534−2542.

(27) Iltchev, N.; Chen, Y. K.; Okada, S.; Yamaki, J. *J. Power Sources* **2003**, *119*, 749−754.

(28) Osorio, A. G.; Silveira, I. C. L.; Bueno, V. L.; Bergmann, C. P. *Appl. Surf. Sci.* **2008**, *255*, 2485−2489.

(29) Streltsov, V. A.; Belokoneva, E. L.; Tsirelson, V. G.; Hansen, N. K. *Acta Crystallogr., Sect. B* **1993**, *49*, 147−153.

(30) Arnold, G.; Garche, J.; Hemmer, R.; Strobele, S.; Vogler, C.; Wohlfahrt-Mehrens, A. *J. Power Sources* **2003**, *119*, 247−251.

(31) Ji, L.; Yao, Y.; Toprakci, O.; Lin, Z.; Liang, Y.; Shi, Q.; Medford, A. J.; Millns, C. R.; Zhang, X. *J. Power Sources* **2010**, *195*, 2050−2056.

(32) Kim, C.; Jeong, Y. I.; Ngoc, B. T. N.; Yang, K. S.; Kojima, M.; Kim, Y. A.; Endo, M.; Lee, J. *Small* **2007**, *3*, 91−95.

(33) Kim, C.; Yang, K. S.; Kojima, M.; Yoshida, K.; Kim, Y. J.; Kim, Y. A.; Endo, M. *Adv. Funct. Mater.* **2006**, *16*, 2393−2397.

(34) Liu, Y.; Pan, C.; Wang, J. *J. Mater. Sci.* **2004**, *39*, 1091−1094.

(35) Morales-Teyssier, O.; Sanchez-Valdes, S.; Ramos-de Valle, L. F. *Macromol. Mater. Eng.* **2006**, *291*, 1547−1555.

(36) Wu, D.; Shi, T.; Yang, T.; Sun, Y.; Zhai, L.; Zhou, W.; Zhang, M.; Zhang, J. *Eur. Polym. J.* **2011**, *47*, 284−293.

(37) Ji, L.; Jung, K.; Medford, A. J.; Zhang, X. *J. Mater. Chem.* **2009**, *19*, 4992−4997.

(38) Ji, L.; Medford, A. J.; Zhang, X. *J. Mater. Chem.* **2009**, *19*, 5593−5601.

(39) Ji, L.; Medford, A. J.; Zhang, X. *Polymer* **2009**, *50*, 605−612.

(40) Li, J.; Ma, P. C.; Chow, W. S.; C., K.; Tang, B. Z.; Kim, J. *Adv. Funct. Mater.* **2007**, *17*, 3207−3215.

(41) Bauhofer, W.; Kovacs, J. Z. *Composites Sci. Technol.* **2009**, *69*, 1486−1498.

(42) Ma, P.; Liu, M.; Zhang, H.; Wang, S.; Wang, R.; Wang, K.; Wong, Y.; Tang, B.; Hong, S.; Paik, K.; Kim, J. *ACS Appl. Mater. Interfaces* **2009**, *1*, 1090−1096.

(43) Gao, F.; Tang, Z. *Electrochim. Acta* **2008**, *53*, 5071−5075.

(44) Liu, H.; Li, C.; Zhang, H. P.; Fu, L. J.; Wu, Y. P.; Wu, H. Q. *J. Power Sources* **2006**, *159*, 717−720.

(45) Park, C. K.; Park, S. B.; Shin, H. C.; Cho, W. I.; Jang, H. *Bull. Korean Chem. Soc.* **2011**, *32*, 191−195.

(46) Chang, C.; Her, L.; Su, H.; Hsu, S.; Yen, Y. T. *J. Electrochem. Soc.* **2011**, *158*, A481−A486.

(47) Zhang, G.; Huang, C.; Zhou, L.; Ye, L.; Li, W.; Huang, H. *Nanoscale* **2011**, *3*, 4174−4181.